Microstructural Characterization of Highly HDS-Active Co_6S_8-Pillared Molybdenum Sulfides

James Brenner, Christopher L. Marshall,* Leroy Ellis,† and Nancy Tomczyk

Argonne National Laboratory, Chemical Technology Division, 9700 South Cass Avenue, Argonne, Illinois 60439-4831

Joy Heising and Mercouri Kanatzidis

Michigan State University, Department of Chemistry and the Center for Fundamental Materials Research, East Lansing, Michigan 48824

Received August 26, 1997. Revised Manuscript Received February 6, 1998

In this work, we have used transmission electron microscopy (TEM) to study $Co_6S_8(PPh_3)_x$-pillared MoS_2 and have directly observed that the Co clusters can either intercalate into the bulk or can bind to defect sites at the edges of MoS_2. A distribution of discrete 0.87 nm scattering centers has been assigned to remnants of the $Co_6S_8(PPh_3)_6$ clusters. On the basis of X-ray diffraction (XRD) studies, a lattice expansion of 1.48 nm was expected if the triphenylphosphine ligands remained intact. The distribution of Co scattering centers, however, was consistent with that expected for a Co_6S_8 core (0.8 nm). The expansion of the $\{00l\}$-MoS_2 planes was almost always localized about a single Co cluster, and the degree of lattice expansion (0.78 nm) was also consistent with the dimensions of the Co_6S_8 cores, confirming that the ligands had been nearly completely removed. The organic ligands were removed either during the vacuum pumpdown in the TEM specimen chamber or almost immediately upon electron-beam exposure. Additional electron-beam exposures of up to 1 h caused no further structural changes. The inorganic framework remained intact throughout the duration of the experiment. The Co_6S_8-pillared MoS_2 materials possessed dibenzothiophene (DBT) hydrodesulfurization (HDS) activities that were slightly better than that of a commercial sulfided Co−Mo/Al_2O_3 catalyst under low-severity HDS conditions. However, the selectivity to biphenyl was somewhat poorer than that of commercial Co−Mo and Ni−Mo catalysts under all conditions examined. The HDS and TEM results suggest that the role of Co in sulfided Co−Mo catalysts is to prop apart MoS_2 layers, creating a higher percentage of "rim" sites (in the Daage−Chianelli terminology) and enhancing hydrogenation capability.

Introduction

Hydrodesulfurization Active Sites Models. Alumina-supported cobalt- and nickel-promoted molybdenum sulfides have been the catalysts of choice for the hydrotreatment of crude oils for several decades. As one progresses from left to right across the periodic table, the HDS activities of transition metal sulfides pass through a maximum near Os and Ir.[2−5] Most commercial hydrotreatment catalysts consist of γ-Al_2O_3-supported Mo or W sulfides promoted with Co or Ni. The activity of these mixed-metal sulfides is substantially greater than the weighted averages of the activities of the monometallic bulk sulfides.

The nature and position of the active sites (Figure 1) in these materials have been a source of much debate for the past 25 years.[6] Several models[1,6−12] have been proposed to explain the promotional effect of Co and Ni on HDS catalysis. These models can be grouped according to the importance of the interaction between Mo (or W) and a late-transition-metal promoter, M (Co, Ni). The anion vacancy and contact synergy models are characterized by weak or indirect interactions between Mo and M.[7−9,12] In contrast, the intercalation and "Co−Mo−S" models are characterized by strong, direct interactions between Mo and M.[6,10−11]

The HDS-active sites, according to the anion vacancy model, are sulfur anion vacancies in a one-dimensional

* To whom correspondence should be addressed.
† Current address: Arco Exploration and Production Technology, Plano, TX.

(1) Daage, M.; Chianelli, R. R. *J. Catal.* **1994**, *149*, 414.
(2) Pecoraro, T. A.; Chianelli, R. R. *J. Catal.* **1981**, *67*, 430.
(3) Vissers, J. P. R.; Groot, C. V.; van Oers, E. M.; deBeer, V. H. J.; Prins, R. *Bull. Chem. Soc. Belg.* **1984**, *93*, 813.
(4) Ledoux, M. J.; Michaux, O.; Agostini, G.; Panissod, P. *J. Catal.* **1986**, *102*, 275.
(5) Lacroix, M.; Boutarfa, N.; Guillard, C.; Vrinat, M.; Breysse, M. *J. Catal.* **1989**, *120*, 473.
(6) Topsøe, H.; Clausen, B. S. *Catal. Rev.-Sci. Eng.* **1984**, *26*, 395.
(7) Lipsch, J. M. J. G.; Schuit, G. C. A. *J. Catal.* **1969**, *15*, 179.
(8) Massoth, F. E. *Adv. Catal.* **1978**, *27*, 265.
(9) Delmon, B. *Prepr. Am. Chem. Soc. Div. Pet. Chem.* **1977**, *22*, 503.
(10) Harris, S.; Chianelli, R. R. *J. Catal.* **1986**, *98*, 17.
(11) DeBeer, V. H. J.; Schuit, G. C. A. In: *Preparation of Catalysts*; Delmon, B., Jacobs, P., Poncelet, G., Eds.; Elsevier Publishers: New York, 1976; p 343.
(12) Vissers, J. P. R.; DeBeer, V. H. J.; Prins, R. *J. Chem. Soc., Faraday Trans. 1* **1987**, *83*, 2145.

S0897-4756(97)00592-9 CCC: $15.00
Published on Web 04/28/1998

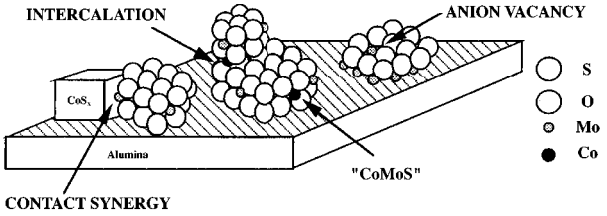

Figure 1. Positions of Co, Mo, and S in hydrodesulfurization (HDS) active site models.[6]

Mo sulfide raft bound to the support.[7−8,13−14] It is believed that the promoter helps stabilize the Mo sulfide chain and increase the number of vacancies.

Delmon[9] proposed that the active sites for HDS are Mo^{3+} ions located at the interface of MoS_2 and Co_9S_8 domains. According to Delmon,[9] the promotional effect of Co on both supported and unsupported MoS_2 catalysts was explained in terms of a "contact synergy" model. This model is based on experiments involving mechanical mixtures of MoS_2 and Co_9S_8 for which a synergistic increase in the activity was observed. It was proposed that the bulk promoter provides sites for hydrogen activation while the Mo sulfide sites utilize this hydrogen to activate aromatic C═S bonds. Inherent in this model is the spillover of hydrogen from the donor (bulk promoter sulfide) to the acceptor (bulk Mo sulfide).

According to the intercalation model, promoter atoms intercalate between layers of MoS_2 crystallites,[11] and the primary function of the promoter is to reduce the Mo oxidation state. Topsøe's "Co−Mo−S" model[6,15] has many similarities with the intercalation model and has gained acceptance over the past decade. Their model, also known as the pseudointercalation or edge-decoration model, was postulated based on a linear relationship between the HDS activity and the amount of Co giving rise to a distinct Mössbauer emission spectroscopy signal assigned to a phase termed "Co−Mo−S".[16−17] Topsøe and Topsøe[18,19] suggested that the amount of NO adsorbed to Co as assessed by infrared spectroscopy (IR) also correlated linearly with HDS activity at low Co loadings (Co/Mo ≤ 0.4). The Mössbauer and IR studies conducted by the Topsøe group represent the best correlations between HDS reactivity in bimetallic sulfide catalysts and either the structural or chemical properties of these catalysts. X-ray absorption spectroscopy results on these same catalysts suggested that Co cations substitute for some Mo atoms along the {002}, or edge, planes of MoS_2.[20] At higher Co loadings (Co/Mo > 0.4), bulk Co_9S_8 domains are formed that do not contribute significantly to HDS activity. These bulk Co_9S_8 domains are not to be confused with the Co_6S_8 molecular cluster cores in this study that are part of the pillars that prop apart the layers of MoS_2.

DeBeer and co-workers were the first to suggest that the late transition metals, long considered to be "promoters" of Mo in sulfide hydrotreatment catalysts, were

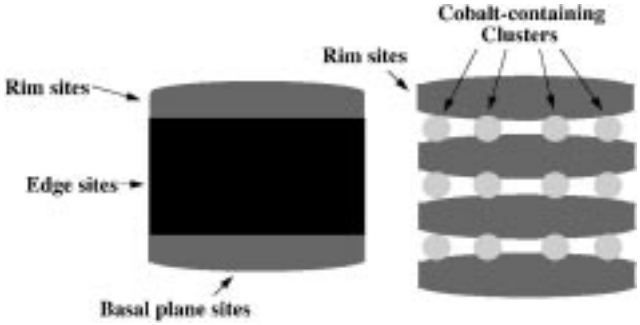

Figure 2. Daage−Chianelli[1] rim-edge model of HDS active sites (left). The Co_6S_8 cluster cores prop apart the MoS_2 layers, effectively creating a higher percentage of "rim" sites and enhancing hydrogenation during HDS.

actually responsible for the catalysis.[12,21−22] This was based upon the following trend in HDS activity: Co/C > Mo/γ-Al_2O_3 > Co/γ-Al_2O_3 > Mo/C (C = activated carbon). Vissers et al.[12] demonstrated that activated carbon was relatively inert as a support compared to γ-Al_2O_3 and concluded that Co complexes with γ-Al_2O_3, forming inactive species.

If Co is the active species, then the Mo sulfide on γ-Al_2O_3 is just a complex support for Co. Evaluation of this hypothesis is perhaps best accomplished by varying the degree of dispersion of the MoS_2. The Mo sulfide component in alumina-supported catalysts prepared by conventional preparation techniques is mostly S−Mo−S single layer sheets. Some of the MoS_2 is multilayered, and the number of MoS_2 layers per particle increases with catalyst age.[23,24]

An alternate way to increase MoS_2 dispersion is to prop open the MoS_2 layers with small Co-containing clusters. For clay materials, this process of propping open sheets is known as pillaring and consists of swelling (or exfoliating) the layered material with a solvent containing a pillaring agent, followed by evacuation of the swelling solution. During the exfoliation of MoS_2, the pillaring process is more complex. A CH_2Cl_2/H_2O emulsion is formed, with species migration across the liquid interface. Also, "exfoliation" of MoS_2 is more like clay delamination, with the major difference being that when clays restack they form a "house-of-cards" structure, whereas with MoS_2 the restacking is more ordered. If prior to the restacking of the MoS_2 layers, one introduces a solution of $Co_6S_8(PPh_3)_6$ in CH_2Cl_2, then the Co-containing clusters act as pillars to prop open the MoS_2 layers.

Daage and Chianelli[1] recently reported a rim-edge model to explain the types of active sites in unpromoted Mo sulfides. If a MoS_2 particle is considered to be a stack of several disks, the "rim" sites are those sites that are associated with edges of the top and bottom disks in the stack, and the "edge" sites are those associated with edges of the disks that are "sandwiched" between the top and bottom disks (Figure 2).[6] According to

(13) Seshadri, K. S.; Massoth, F. E.; Petrakis, L. *J. Catal.* **1970**, *19*, 95.
(14) Massoth, F. E. *J. Catal.* **1977**, *50*, 190.
(15) Topsøe, H.; Clausen, B. S.; Candia, R.; Wivel, C.; Mørup, S. *J. Catal.* **1981**, *68*, 433.
(16) Wivel, C.; Candia, R.; Clausen, B. S.; Mørup, S.; Topsøe, H. *J. Catal.* **1981**, *68*, 453.
(17) Mørup, S.; Clausen, B.; Topsøe, H. *J. Phys.* **1979**, *40 (C2)*, 88.
(18) Topsøe, N.-Y.; Topsøe, H. *J. Catal.* **1982**, *77*, 293.
(19) Topsøe, N.-Y.; Topsøe, H. *J. Catal.* **1983**, *84*, 386.
(20) Clausen, B. S.; Topsøe, H.; Candia, R.; Villadsen, J.; Lengeler, B.; Als-Nielsen, J.; Christensen, F. *J. Phys. Chem.* **1981**, *85*, 3868.
(21) DeBeer, V. H. J.; Duchet, J. C.; Prins, R. *J. Catal.* **1981**, *72*, 369.
(22) Duchet, J. C., Van Oers, E. M.; DeBeer, V. H. J.; Prins, R. *J. Catal.* **1983**, *80*, 386.
(23) Eijsbouts, S.; Inoue, Y. *Stud. Surf. Sci. Catal.* **1995**, *92*, 429.
(24) Eijsbouts, S.; VanLeerdam, G. C. *Bull. Soc. Chim. Belg.* **1995**, *104*, 347.

Daage and Chianelli, the rim sites are capable of both HDS and HYD (hydrogenation), whereas the edge sites are capable only of HDS. One way to evaluate the validity of Daage and Chianelli's rim-edge model would be to exfoliate the MoS_2 in the absence of a pillaring agent. One would expect that an exfoliated and flocculated material would contain a higher density of rim sites because the exfoliation/flocculation process increases the basal plane area and hence increases the surface area of MoS_2. Thus, restacked MoS_2 would be expected to be more active but less selective than a nonexfoliated MoS_2 for direct desulfurization of dibenzothiophene to biphenyl. Unfortunately, the rim-edge model does not address the effects of Co or Ni.

Pillared Chalcogenides. Interest in the possibility of generating microporous chalcogenides has been increasing during the past few years,[25−36] particularly in the field of electronic materials. Several groups, particularly those of Chianelli,[37] Frindt,[38] Nazar,[39−41] Fuentes,[42] Curtis,[43] and Wypych[44] have exfoliated Li_xMoS_2 in H_2O to form a restacked MoS_2, usually with surface areas of 10 m^2/g but occasionally as high as 50 m^2/g and much higher than the 5−6 m^2/g MoS_2 obtainable from commercial vendors. Several reports,[39−41,43,45] particularly those of Nazar, have appeared recently on the subject of pillared layered chalcogenides as well. Not until the preparation of this paper had intercalated chalcogenides been tested for hydrodesulfurization activity, however. Curtis[43] and co-workers will soon report on materials prepared by exfoliation of Li_xMoS_2 in H_2O followed by flocculation in solutions of simple Co hydrate, Co amine, and Co cyclopentadienyl complexes. These materials exhibit thiophene HDS activities comparable to conventionally prepared Co−Mo sulfides, but the Co complexes deintercalate during HDS.

Recently, we reported a new family of materials based on layered transition-metal dichalcogenides of the type $[Co_6Q_8(PR_3)_n]_xMS_2$ (Q = S, Se, Te; M = Mo, W; R = alkyl, phenyl) prepared as a first step toward pillared layered sulfides.[46] The pillars in these materials are the cuboidal $Co_6S_8(PR_3)_6$ clusters. The $[Co_6S_8(PR_3)_n]_x$-MoS_2 materials are of particular interest in HDS catalysis because they are compositionally similar to the commercial "Co−Mo−S" catalysts and simultaneously represent a structural arrangement between the Co and Mo centers which is different than previously studied. The pillaring process increases the surface area and, thus, may increase the dispersion of potentially active centers. Therefore, the $[Co_6S_8(PR_3)_n]_xMoS_2$ family of compounds presents a unique opportunity to also probe several mechanistic HDS models. In this work, we have directly observed the presence of discrete cobalt-containing entities in the bulk MoS_2 lattice and along $\{00l\}$-MoS_2 planes in an HDS-active material; in addition, the Co_6S_8 cluster fragments appear to stay within the MoS_2 lattice during HDS.

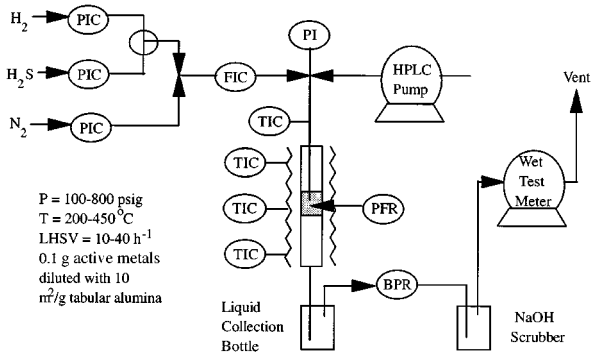

Figure 3. Pilot plant scale HDS catalytic reactor schematic. PIC = pressure indicating controller, FIC = flow indicating (mass flow controller), PFR = plug flow reactor, BPR = back pressure regulator, and PI = pressure indicator (transducer).

Table 1. HDS Pilot Plant Operating Conditions

liquid velocity = 0.25 g/min	pressure = 400 psig
gas velocity = 700 cm^3/min.	preheater temp = 350 °C
$H_2/H_2S/N_2$ = 5/0/2	furnace temp = 300−400 °C
catalyst loading = 0.10 g metal	tabular alumina diluent = 2.5−3.0 g

liquid feed = 1.0 wt % S as DBT in *n*-C_{16} (normal hexadecane, *n*-$C_{16}H_{34}$; Aldrich Chemical)

Experimental Section

Materials Preparation. $LiMoS_2$ was prepared using procedures developed previously[46] (in 0.25 g batches) under nitrogen in dried Schlenkware using one of two methods described below:

(A) After drying 2H−MoS_2 (Aldrich Chemical, 99+%) under vacuum overnight, the flask was placed under a nitrogen atmosphere. Hexane was refluxed, distilled over CaH_2, and then used to dilute 2.4 M *n*-BuLi (Aldrich) to 1.0−1.6 M. After stirring at least a 3-fold molar excess of *n*-BuLi with the 2H−MoS_2 for 3 days, the solution was poured under positive N_2 pressure through a Schlenk frit, filtered under N_2, and rinsed with copious amounts of hexane to remove byproducts and unreacted starting material.

(B) 2H−MoS_2 was ground in a N_2 atmosphere glovebox with a 2.5 molar excess of $LiBH_4$ and then placed in a quartz tube. The resulting material was heated in a furnace to 300 °C for

(25) Bedard, R. L.; Wilson, S. T.; Vail, L. D.; Bennett, E. M.; Flanigen, E. M. In: *Zeolites: Facts, Figures, Future*; Jacobs, P. A., van Santen, R. A., Eds.; Elsevier Science Publishers B. V.: Amsterdam, The Netherlands, 1989; pp 375−387.
(26) Bedard, R. L.; Vail, L. D.; Wilson, S. T.; Flanigen, E. M. U.S. Patent 4,880,761 1989.
(27) Parise, J. B. *Science* **1991**, *251*, 293.
(28) Ko, Y.; Tan, K.; Nellis, D. M.; Koch, S.; Parise, J. B. *J. Solid State Chem.* **1995**, *114*, 506.
(29) Dhingra, S.; Kanatzidis, M. G. *Science* **1992**, *258*, 1769.
(30) Kim, K.-W.; Kanatzidis, M. G. *J. Am. Chem. Soc.* **1992**, *114*, 4878.
(31) Kim, K.-W.; Kanatzidis, M. G. *Inorg. Chem.* **1991**, *30*, 1966.
(32) Marking, G. A.; Kanatzidis, M. G. *Chem. Mater.* **1995**, *7*, 1915.
(33) Ozin, G. A. *Adv. Mater.* **1992**, *4*, 612.
(34) Enzel, P.; Henderson, G. S.; Ozin, G. A.; Bedard, R. L. *Adv. Mater.* **1995**, *7*, 64.
(35) Jiang, T.; Lough, A. J.; Ozin, G. A.; Young, D. *Chem. Mater.* **1995**, *7*, 245.
(36) Enzel, P.; Henderson, G. S.; Ozin, G. A.; Bedard, R. L. *Adv. Mater.* **1995**, *7*, 166.
(37) Chianelli, R. R. *Catal. Rev.-Sci. Eng.* **1984**, *26*, 361.
(38) Yang, D.; Sandoval, S. J.; Divigalpitiya, W. M. R.; Irwin, J. C.; Frindt, R. F. *Phys. Rev. B* **1991**, *43*, 12053.
(39) Nazar, L. F.; Yin, X. T.; Zinkweg, D.; Zhang, Z.; Liblong, S. *Mater. Res. Soc. Symp. Proc.* **1991**, *210*, 417.
(40) Nazar, L. F.; Jacobson, A. J. *J. Chem. Soc., Chem. Commun.* **1986**, 570.
(41) Nazar, L. F.; Jacobson, A. J. *J. Mater. Chem.* **1994**, *4*, 149.
(42) del Valle, M.; Avalos-Borja, M.; Cruz, J.; Fuentes, S. *Mater. Res. Soc. Symp. Proc.* **1994**, *351*, 287.
(43) Dungey, K. E.; Curtis, M. D.; Penner-Hahn, J. E. *J. Catal.*, submitted.
(44) Wypych, F.; Schollhorn, R. *J. Chem. Soc., Chem. Commun.* ***1992***, 1386.
(45) Lerf, A.; Lalik, E.; Kolodziejski, W.; Klinowski, J. *J. Phys. Chem.* **1992**, *96*, 7389.
(46) Bissessur, R.; Heising, J.; Hirpo, W.; Kanatzidis, M. G. *Chem. Mater.* **1996**, *8*, 318.

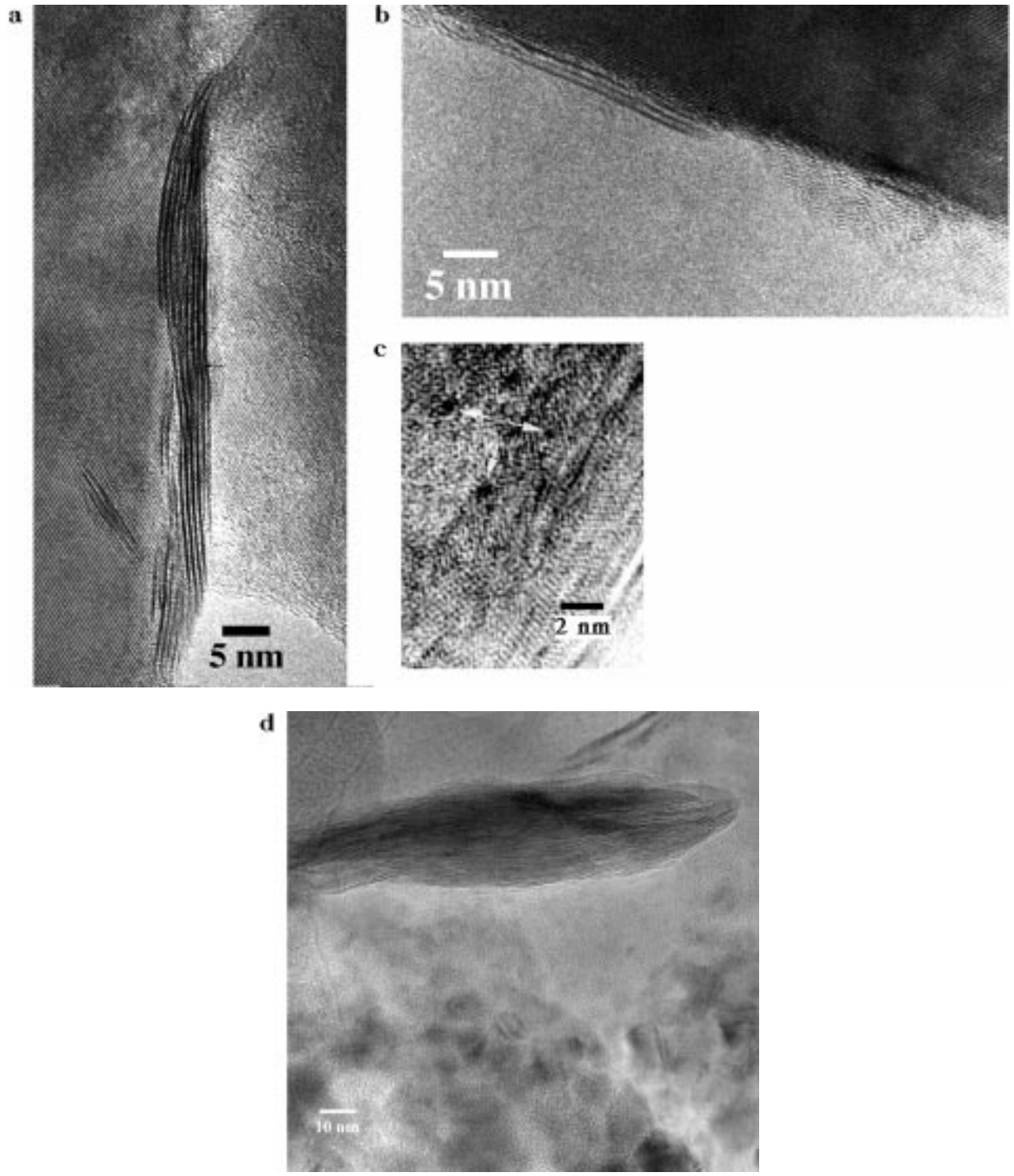

Figure 4. Regions from (a) pristine MoS_2, (b) restacked MoS_2, (c) $[Co_6S_8(PPh_3)_n]_{0.02}MoS_2$, and (d) 0.05-$[Co_6S_8(PPh_3)_n]$−$MoS_2$−R. Exfoliation and solvent evacuation decreases the range of order of the MoS_2 (Figure 4C), but not until the Co-containing clusters are added are there any observations of either lattice expansion or discrete scattering centers. Addition of the Co-containing clusters to the lower surfacearea restacked MoS_2 (Figure 4D) results in a significant segregation of Co into large Co-rich domains (spheres in the bottom of the micrograph).

3 days, during which time the tube was periodically vented to relieve buildup of gaseous byproducts.

$LiMoS_2$ exfoliates in water via a redox reaction, generating LiOH and H_2. After exfoliation of the resulting $LiMoS_2$ in water,[2,37−45] centrifugation, and washing three times to remove excess LiOH (final pH ∼ 7), the $[Co_6S_8(PPh_3)_n]_xMoS_2$ materials were then prepared via the addition of a CH_2Cl_2 solution of $Co_6S_8(PPh_3)_6$[47−50] to the aqueous, exfoliated suspension of MoS_2 (1:40 or 1:20 molar ratio of cluster to MoS_2; $x = 0.025$ or 0.050 by molar ratio, respectively). Values of $x = 0.02$ and 0.05 in $[Co_6S_8(PPh_3)_n]_xMoS_2$ were determined by elemental analysis, respectively.[46] After 2 days of stirring, the MoS_2 flocculated, encapsulating the clusters and collecting at the interface between the solvents. The products were isolated by vacuum filtration and washed with CH_2Cl_2 to remove any external cluster. The products were then dried under vacuum overnight. For comparison purposes, an $Al_{13}O_4(OH)_{24}(H_2O)_{12}^{7+}$-pillared material[51] was prepared by substituting $Al_{13}O_4(OH)_{24}$-

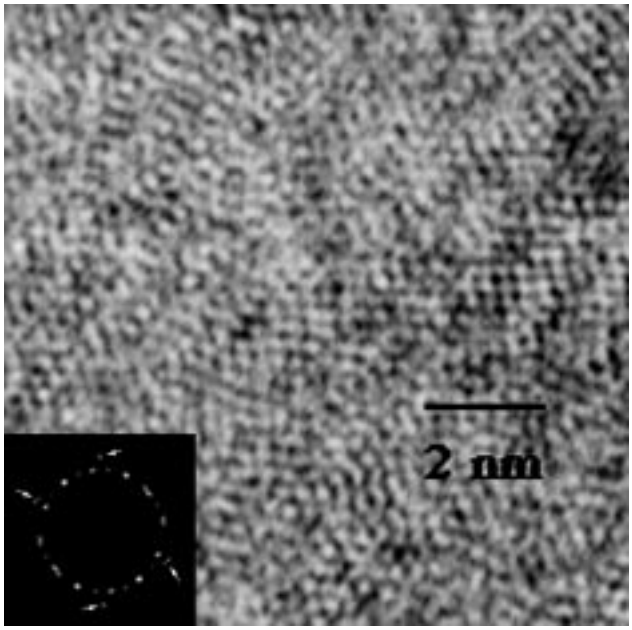

Figure 5. Unpillared {100} regions of $[Co_6S_8(PPh_3)_n]_{0.02}MoS_2$ containing both 1T−MoS_2 and 2H−MoS_2 with optical diffractogram associated with Figure 5. The ring of spots is associated with the {100}-1T−MoS_2 planes. The few spots slightly further away from the center of the diffraction patterns (indicated by white arrows) correspond to {100}-2H−MoS_2.

$(H_2O)_{12}^{7+}$ for $Co_6S_8(PPh_3)_6$ during the intercalation step.

To deconvolute the effects of structural and electronic promotional effects of the $Co_6S_8(PPh_3)_6$ clusters on MoS_2, two additional reference samples *x*-$[Co_6S_8(PPh_3)_n]$−MoS_2−R (*x* = 0.02 and 0.05, R = reference) were prepared. For these materials, the MoS_2 layers were restacked prior to the addition of the Co-containing clusters. Because the MoS_2 layers were restacked prior to addition of the $Co_6S_8(PPh_3)_6$ clusters, and because of the relatively low surface area of the restacked material (10 m^2/g), intercalation of the $Co_6S_8(PPh_3)_6$ into the MoS_2 layers would not be expected to take place. As a result, the morphology of these reference materials would parallel Topsøe's edge-decoration model,[6,15] if the Co-containing clusters did not aggregate. If the Co_6S_8 in the *x*-$[Co_6S_8(PPh_3)_n]$−MoS_2−R materials segregated into large, distinct Co_xS_y domains and if any promotional effect for Co on the HDS activity of MoS_2 was exhibited in these materials, such results would support Delmon's "contact synergy" hypothesis.[9] In this hypothesis, Delmon claims that the most active HDS sites lie at the interface between Co_9S_8 and MoS_2 domains. The synthesis of the Co-containing reference materials consisted of exfoliating $LiMoS_2$, washing twice (by centrifuging, decanting the supernatant, and adding fresh deionized H_2O) to remove the LiOH generated upon exfoliation, and drying the product on a glass slide to yield restacked MoS_2 in 85% yield. After dissolving the $Co_6S_8(PPh_3)_6$ cluster in CH_2Cl_2, the resulting solution was added to the MoS_2 powder and stirred at room temperature in an open Erlenmeyer flask in the hood until the solvent was evaporated. After adding more solvent and evaporating the additional solvent, the product was stored under N_2 until further use.

Prior to use as a catalyst, the $[Co_6S_8(PPh_3)_n]_xMoS_2$ materials were purged in N_2 at 20 °C for 30 min at 1000 cm^3/min, dried in N_2 at 150 °C for 60 min and at 200 °C for 60 min, and then reduced in H_2 for 2 h at 200 °C. Subsequent runs were conducted after prereduction at 250, 300, and 400 °C and after presulfiding in 8% H_2S/H_2 at 300 °C. No substantial differences were observed between the activities after reduction and/or presulfiding. Commercially available oxidized Co−Mo (Crosfield 465) and Ni−Mo (Crosfield 504) were purged in N_2 at 20 °C for 30 min at 1000 cm^3/min, dried in N_2 at 150 °C for 60 min and at 400 °C for 60 min, and finally sulfided in a 8% H_2S/H_2 at 400 °C mixture prior to use.

Transmission Electron Microscopy. Approximately 0.01 g of fresh $[Co_6S_8(PPh_3)_n]_xMoS_2$ was placed into a vial containing ~3 mL of 2-propanol. After sonicating for 30 min, several drops of the resulting slurry were pipetted onto 3 mm holey carbon on Cu grids. Once dry, the grids were inserted into nontilt holders and loaded into a JEOL 4000EX II (line-to-line resolution = 0.14 nm, point-to-point resolution = 0.17 nm). The micrographs were in all cases taken at magnifications of either 150000× or 500000×. The morphologies of the $[Co_6S_8(PPh_3)_n]_xMoS_2$ materials were not noticeably affected by exposure to the 2-propanol when compared to the materials prepared by dipping the grids into the $[Co_6S_8(PPh_3)_n]_xMoS_2$ powder.

After scanning in the micrographs at 400 dpi using an Epson ES-1000C scanner, the measuring tool function in NIH Image 1.59 was used to determine the particle diameters. The distances have been referenced to those for the {001}-1T-MoS_2

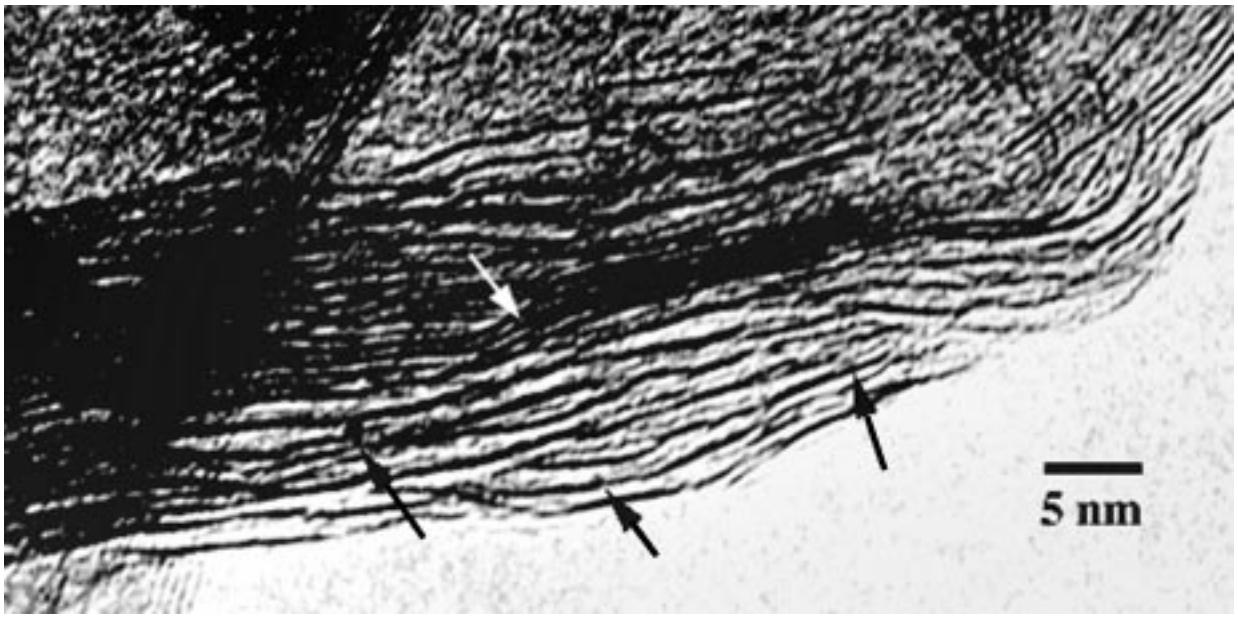

Figure 6. This region of the $[Co_6S_8(PPh_3)_n]_{0.02}MoS_2$ appeared to be nearly completely pillared and partially delaminated, although a section within the same particle (white arrow) was not intercalated at all. Black arrows indicate scattering centers of 0.5−1.5 nm in diameter.

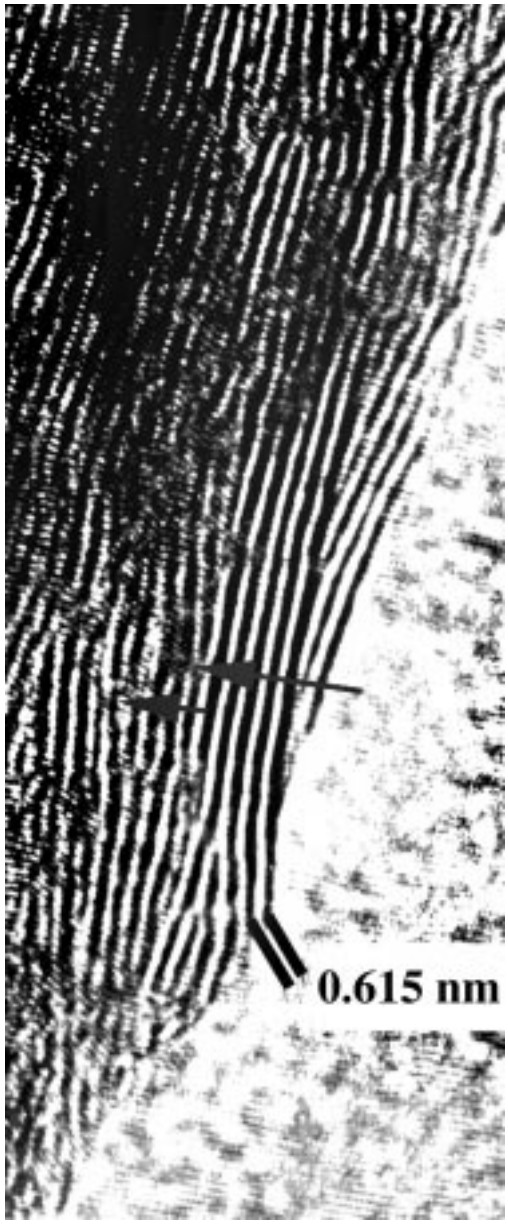

Figure 7. Arrows indicate local disruptions in the MoS_2 edge planes of approximately 0.9 nm diameter in the $[Co_6S_8(PPh_3)_n]_{0.02}MoS_2$ material.

(c = 0.615 nm, ref 38) examined at 500000× and scanned in at 600 dpi. Scale markers placed on the micrographs are approximate.

Catalytic HDS Testing. The pilot plant scale HDS unit shown schematically in Figure 3 was constructed with the help of Dr. John Young of EC Technologies. The reactor consisted of a thick-walled 0.375 in. i.d. 316 SS tube, with the catalyst diluted with a nonporous tabular alumina (LaRoche T-1061) sitting between plugs of quartz wool. Beneath the lower plug was a 0.125 in. i.d., 0.375 in. o.d. deadman used to minimize volume between the reactor and the liquid receiver. Typical conditions for catalytic testing are summarized in Table 1. These conditions were chosen so as to mimic those of an industrial middle distillate desulfurization unit. The weight loadings of the Co_6S_8-pillared MoS_2 materials (0.1 g) and the commercial catalysts (1.0 g) have been adjusted so as to make the total metal (Co or Ni + Mo) loadings equivalent.

The liquid products (typically 60 g at 15 g/h per temperature) were weighed for later determination of mass balance closure (95−102%). A small aliquot (∼1 g) and a vial (∼20 g) of product was saved each hour for later analysis. From the small aliquot, 100 mg of product was diluted to 10 mL with hexane, of which 30 μL was diluted further with hexane to 1.00 mL for GC-MS analysis. The diluted products were separated using a DB5-MS column and analyzed using an HP 5890 GC-MS Series II Plus. Random errors associated with GC-MS concentration measurements were less than 5% of the reported values, and the reproducibility of activity measurements was ±15%. The percentage conversions consistently leveled off after less than 2 h time-on-stream. Selectivity is defined as the percentage of biphenyl yield divided by the dibenzothiophene conversion.

Results

Transmission Electron Microscopy. The pristine MoS_2 was composed of highly ordered crystals (Figure 4a). Exfoliation of the MoS_2, followed by evacuation of H_2O solvent, increased the MoS_2 surface area and shortened the length scale for MoS_2 ordering, but substantial MoS_2 order still remained. In neither the pristine nor restacked MoS_2 materials (Figure 4b) were any discrete scattering centers observed, and the number of dislocation faults was relatively low. In contrast to the materials that contained no cobalt clusters, dispersed among the $\{hk0\}$-MoS_2 planes found in the $[Co_6S_8(PPh_3)_n]_{0.02}MoS_2$ were some discrete scattering centers of weak intensity (Figure 4c) of 0.5−1.5 nm in diameter. The Co-containing species in the x-$[Co_6S_8(PPh_3)_n]$−MoS_2−R materials distinctly segregated into large, Co-rich domains (Figure 4d).

The microstructure of the Co_6S_8-intercalated MoS_2 material consisted of crystal facets containing the following types of planes: $\{001\}$-$[Co_6S_8(PPh_3)_n]_{0.02}MoS_2$, $\{001\}$-1T-MoS_2, $\{hk0\}$-1T-MoS_2, $\{002\}$-2H−MoS_2, and $\{hk0\}$-2H−MoS_2. The 1T and 2H forms of MoS_2 cannot be distinguished clearly by the $\{00l\}$ spacings but can be distinguished by their $\{hk0\}$planes.

Figure 5 is an image and optical diffraction pattern obtained by Fourier transform, respectively, of a representative region of $[Co_6S_8(PPh_3)_n]_{0.02}MoS_2$ containing $\{hk0\}$, or basal, planes. The inner ring of brighter spots correspond to the $\{hk0\}$-1T−MoS_2 planes (a = 0.327 nm), and the few faint spots slightly further away from the center of the diffraction are associated with $\{hk0\}$-2H−MoS_2 planes (a = 0.316 nm). The relative intensities suggested that the percentage of 2H−MoS_2 in this material, while present, was low. X-ray diffraction of a freshly restacked material[46] appears to contain only one phase, 1T−MoS_2, but this phase is transformed with heat, pressure, or time to the 2H form.[46]

The region of $[Co_6S_8(PPh_3)_n]_{0.02}MoS_2$ in Figure 6 appeared to be nearly completely pillared and partially delaminated, although a section within the same particle (white arrow) was not intercalated at all. This was the only region for which lattice expansion was continuous over any distance longer than a single $Co_6S_8(PPh_3)_6$ cluster in the low-loaded $[Co_6S_8(PPh_3)_n]_{0.02}MoS_2$ material. Here, the distance between the layers which were

(47) Stuczynski, S. M.; Kwon, Y.-U.; Steigerwald, M. L. *J. Organomet. Chem.* **1993**, *449*, 167.
(48) Steigerwald, M. L.; Siegrist, T.; Stuczynski, S. M. *Inorg. Chem.* **1991**, *30*, 4940.
(49) Hong, M.; Huang, Z.; Lei, X.; Wei, G.; Kang, B.; Liu, H. *Polyhedron* **1991**, *10*, 927.
(50) Hong, M.; Huang, Z.; Lei, X.; Wei, G.; Kang, B.; Liu, H. *Inorg. Chim. Acta* **1989**, *159*, 1.
(51) Heising, J.; Bonhomme, F.; Kanatzidis, M. G. *J. Solid State Chem.*, in press.

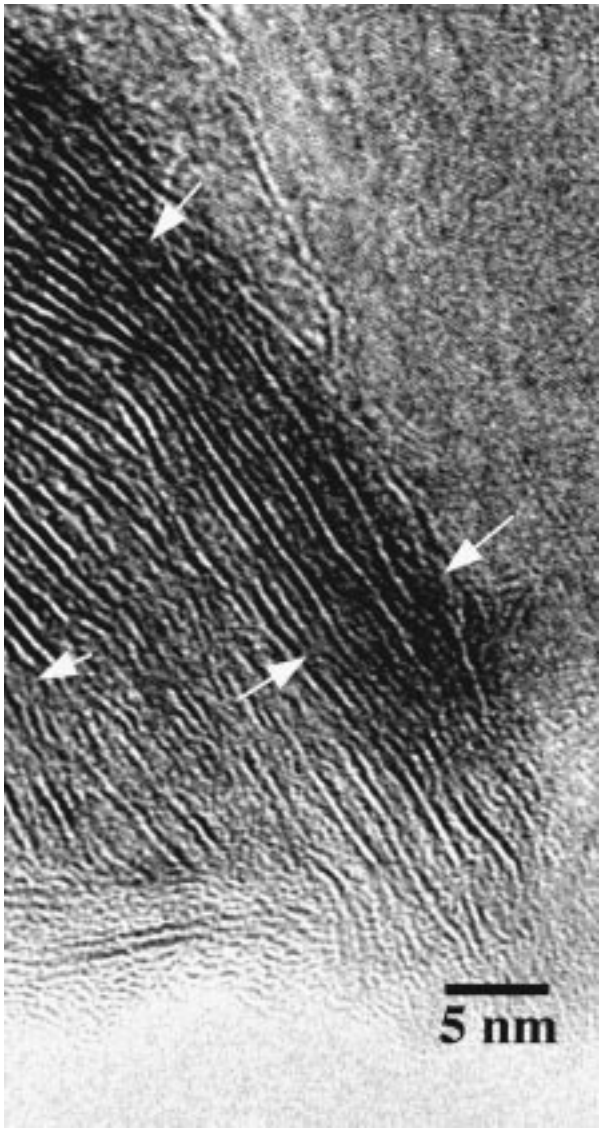

Figure 8. Arrows indicate local disruptions in the MoS_2 edge planes of approximately 0.9 nm diameter in the $[Co_6S_8(PPh_3)_n]_{0.02}MoS_2$ material.

obviously pillared was 1.39 ± 0.10 nm. Arrows indicate scattering centers of 0.5−1.5 nm in diameter.

Several micrographs of the $[Co_6S_8(PPh_3)_n]_{0.02}MoS_2$ material appeared very similar to those reported for unintercalated MoS_2; however, upon closer inspection, the material was composed of locally disturbed MoS_2 layers. Arrows in Figures 7 and 8 point to local disruptions in the {001}-1T−MoS_2 planes.

The size distribution of the discrete scattering centers has been summarized in Figure 9 and Table 2. This distribution was constructed by grouping the data into logarithmically evenly spaced bins ranging from 0.17 to 100 nm. The smallest of these scattering centers was 0.32 nm, barely above our ability to confidently assign such a feature as real. Scattering centers greater than 0.40 nm are certainly real. The size distribution of scattering centers was fitted with a log-normal distribution using the commercially available program PeakFit (Jandel Scientific). The particle size distribution data (points), the computer fit of the data (solid line), and the 95% prediction intervals (dashed lines) have been reported. This 95% prediction interval defines the

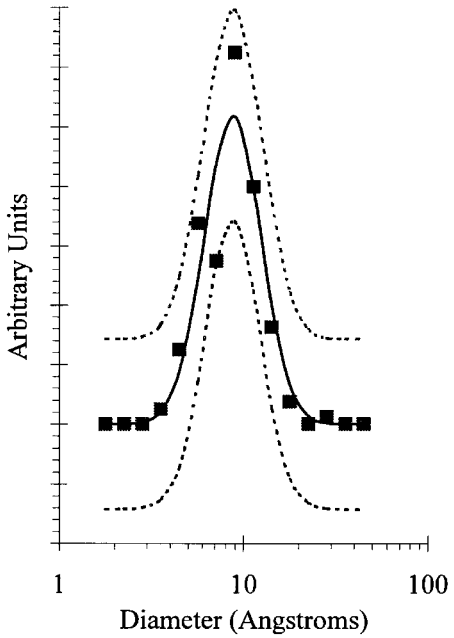

Figure 9. Size distribution of scattering centers in Co_6S_8-pillared MoS_2 observed by TEM.

Table 2. TEM Size Distribution of Cobalt Clusters[a]

material	log mean (nm)	fwhm (nm)	no. of scatterers
$[Co_6S_8(PPh_3)_n]_{0.02}MoS_2$	0.87 ± 0.03	0.75 ± 0.08	160
$[Co_6S_8(PPh_3)_n]_{0.02}MoS_2$ used	0.94 ± 0.06	0.85 ± 0.10	79
$[Co_6S_8(PPh_3)_n]_{0.05}MoS_2$	0.92 ± 0.07	0.90 ± 0.15	53

[a] Reported errors are standard deviations.

confidence interval for an individual curve fit. Thus, one would expect that 95 out of 100 individual curve fits would fall within the 95% prediction interval. The abscissa of this histogram has been scaled logarithmically to make the particle size distribution appear Gaussian.

Representative regions of the $[Co_6S_8(PPh_3)_n]_{0.05}MoS_2$ material appeared quite similar to that observed for the $[Co_6S_8(PPh_3)_n]_{0.02}MoS_2$. As in Figures 7 and 8, local disruptions in the {00*l*}-1T−MoS_2 planes (Figure 10) as well as lattice expansions of about 0.9 nm (Figure 11) were common. In the $[Co_6S_8(PPh_3)_n]_{0.05}MoS_2$ material, the higher loading of Co sometimes resulted in some slightly larger Co_xS_y aggregates at the external surface of MoS_2 (Figure 10) as well as longer range pillaring of the MoS_2 layers. Expulsion and subsequent aggregation of the Co_6S_8 guests from octahedral 1T−MoS_2 occurred concomitantly with the conversion to 2H−MoS_2. Such guest expulsion has also been observed for other $[Co_6Q_8(PR_3)_n]_xMS_2$ (Q = S, Se, Te; M = Mo, W; R = alkyl, phenyl) systems.[46]

Catalytic materials often change during or after use. Figure 12 displays a typical micrograph of the $[Co_6S_8(PPh_3)_n]_{0.02}MoS_2$ material after use as an HDS catalyst. The degree of Co_6S_8 pillaring remained relatively constant. The lattice expansion of the MoS_2 edge planes appeared to be slightly higher than the expansion before use as a catalyst (0.85 vs 0.78 nm), but certainly this difference is within the experimental error of the measurements. Likewise, it is difficult to say whether the increase in the log-mean diameter of the scattering centers (from 0.87 nm before use to 0.94 nm after use)

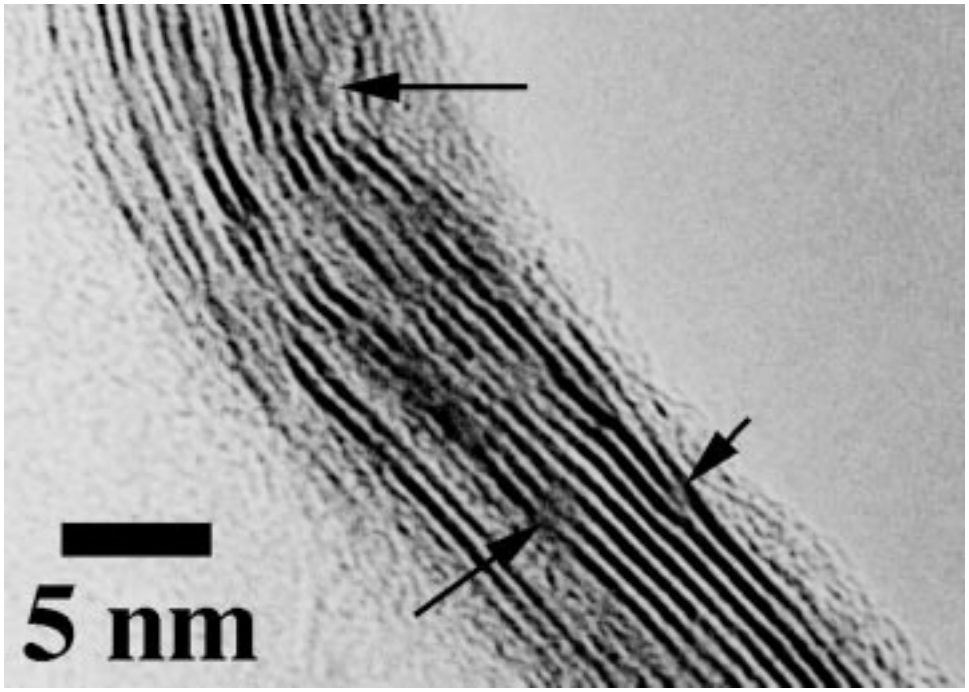

Figure 10. Edge planes in the $[Co_6S_8(PPh_3)_n]_{0.05}MoS_2$ material contain even more local disruptions of approximately 1.0 nm in diameter than the $[Co_6S_8(PPh_3)_n]_{0.02}MoS_2$ material.

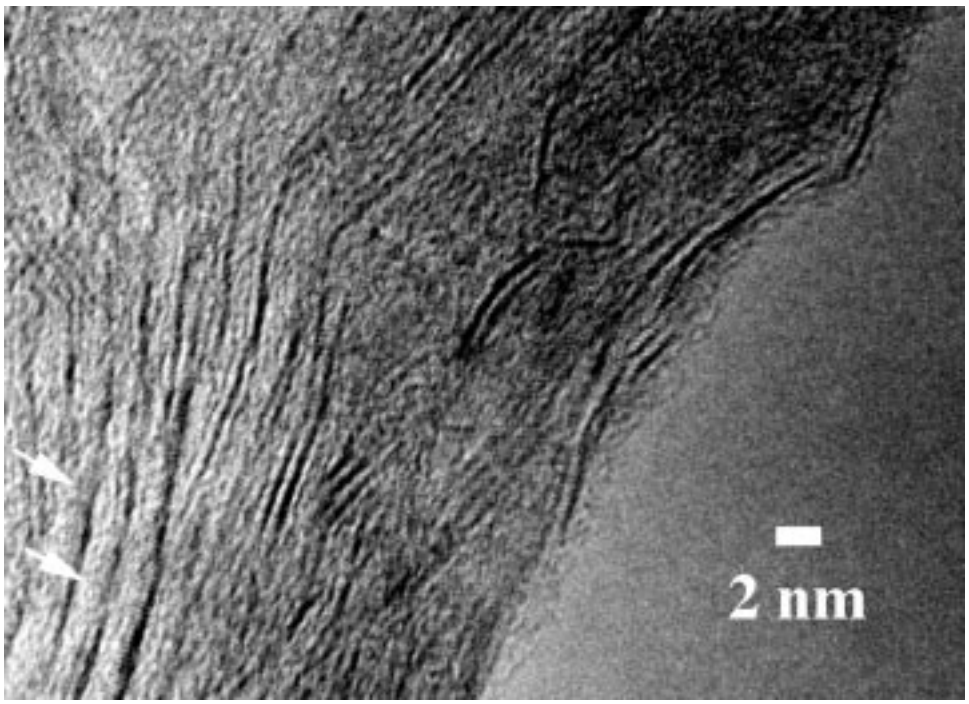

Figure 11. Percentage of completely pillared and partially delaminated layers of $[Co_6S_8(PPh_3)_n]_{0.05}MoS_2$ increases with Co cluster loading.

attributed to the Co_6S_8 cluster cores was significant. Therefore, from these results, it can be concluded that the Co_6S_8 cluster core pillars remain essentially intact with respect to HDS.

Figures 13 and 14 show the same region of the $[Co_6S_8(PPh_3)_n]_{0.02}MoS_2$ material after 2 min and after 1 h of electron-beam exposure at 20 pA/cm^2. There were no substantial differences in the region. Thus, after the first 2 min, there was no detectable electron-beam damage. Electron-beam degradation of the organic ligands during the first 2 min cannot be ruled out, however. The inorganic framework was stable throughout the duration of the experiment.

HDS Activity. Hydrodesulfurization activities for the Co_6S_8-pillared MoS_2 and the commercially available sulfided, promoted Mo catalysts were severely mass-transfer limited at all liquid hourly space velocities tested, at temperatures below 350 °C (Table 3). In the absence of mass-transport limitations, activity should be independent of liquid hourly space velocity (LHSV).

(52) Brenner, J.; Thiyagarajan, P.; Ellis, L.; Anderson, K.; Tomczyk, N.; Marshall, C.; Winans, R., to be submitted to *Energy Fuels*.

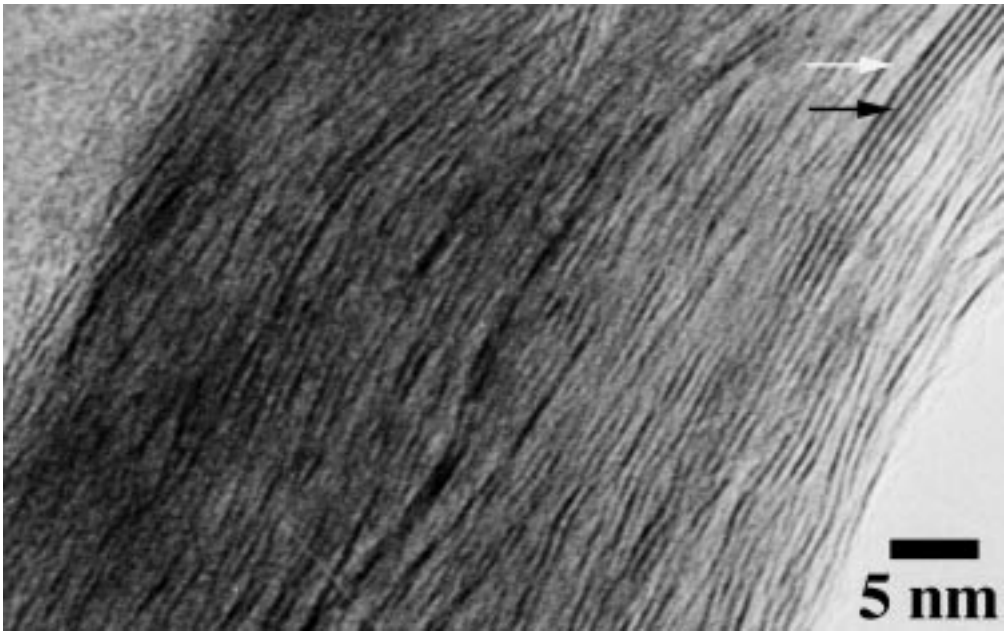

Figure 12. Significant degree of pillaring remains in the $[Co_6S_8(PPh_3)_n]_{0.02}MoS_2$ material after use as an HDS catalyst. The lattice constant for the pillared MoS_2 materials remains constant within experimental error before and after catalysis.

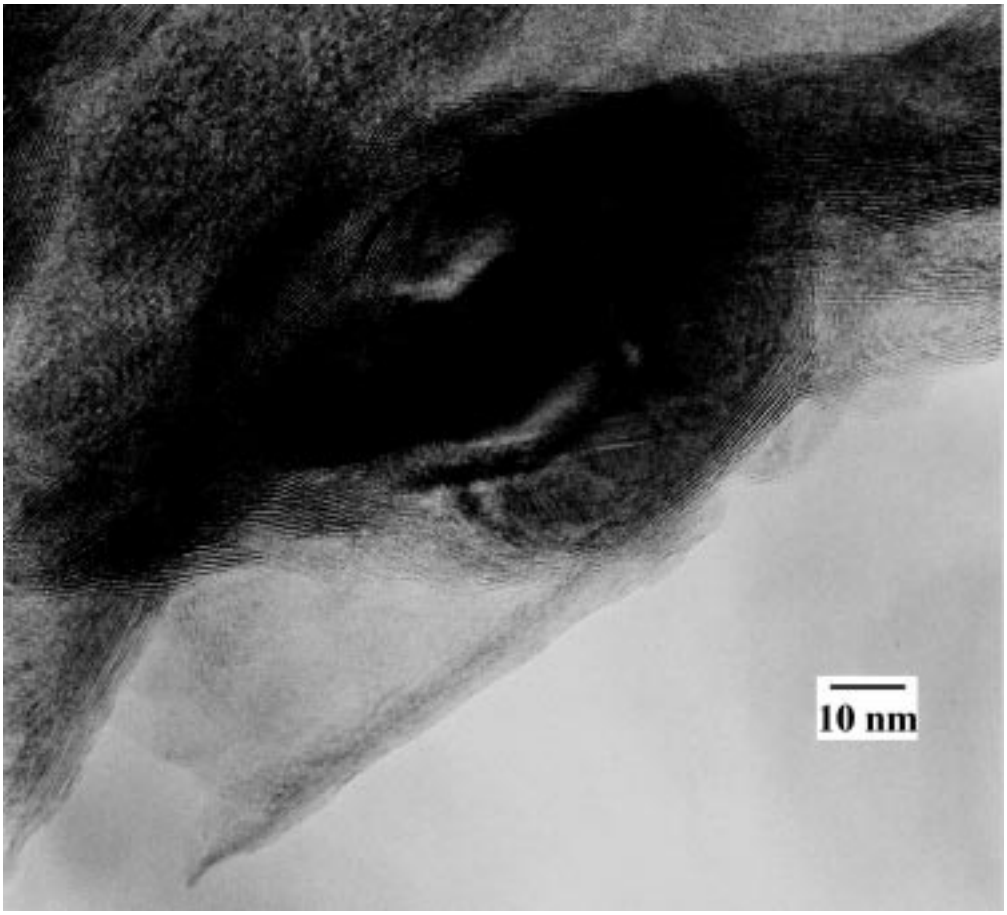

Figure 13. Region from $[Co_6S_8(PPh_3)_n]_{0.02}MoS_2$ after an electron-beam exposure of 2 min at 20 pA/cm^2.

Mass-transport limitations were not nearly so dramatic at or above 350 °C, where industrial hydrotreating units typically operate. We have observed this trend for a wide variety of catalysts.[52]

Despite the mass transport limitations, the Co_6S_8-pillared MoS_2 materials possessed higher dibenzothiophene HDS activities than commercial, sulfided Co−Mo and Ni−Mo catalysts at 300 °C and below. Most of this high activity could be attributed to enhanced hydrogenation functionality as indicated by the relatively low selectivities to biphenyl. Biphenyl is the desired, direct desulfurization (C═S bond cleavage) product from dibenzothiophene. The other primary reaction pathway proceeds through saturation of one of

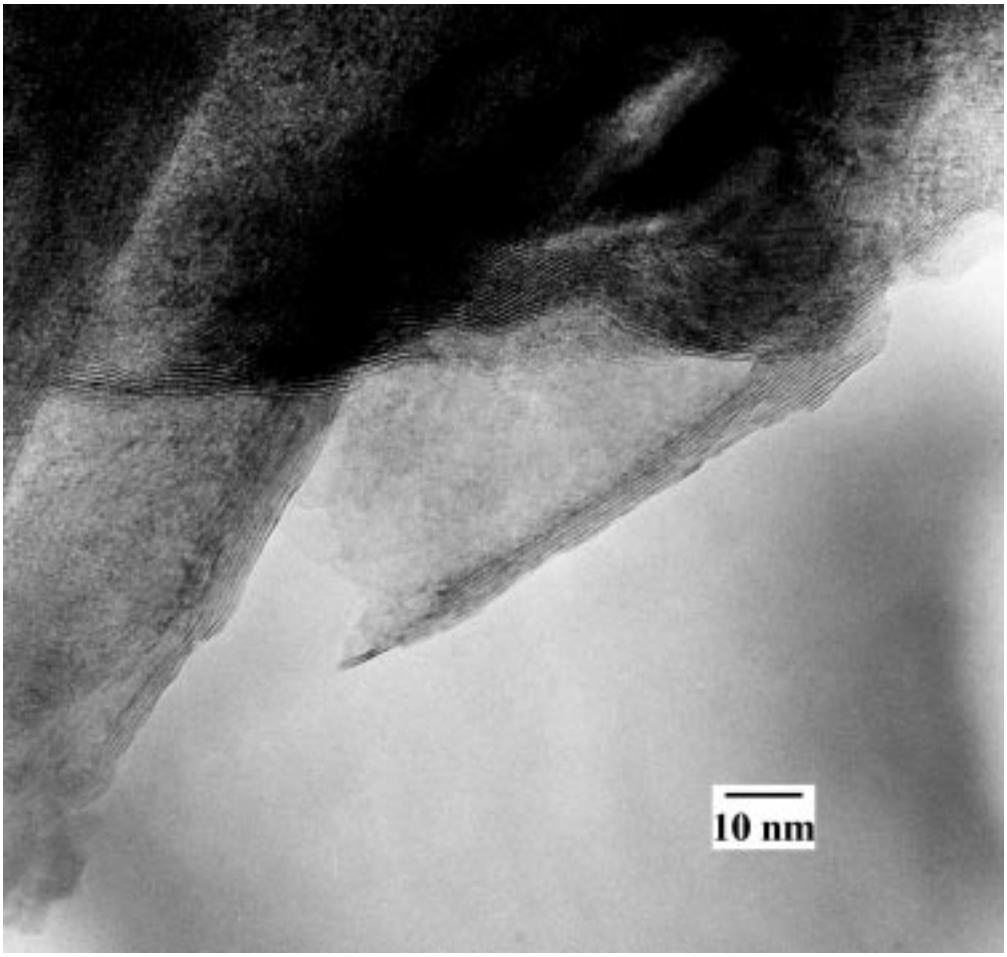

Figure 14. Region of $[Co_6S_8(PPh_3)_n]_{0.02}MoS_2$ shown in Figure 14 after an electron- beam exposure of 1 h at 20 pA/cm^2.

Table 3. Mass Transport Limitations[a]

	catalyst											
	$[Co_6S_8(PPh_3)_n]_{0.02}MoS_2$				Crosfield 465 (Co−Mo)				Crosfield 504 (Ni−Mo)			
LHSV (h^{-1})	5	10	20	40	5	10	20	40	5	10	20	40
% conversion at 300 °C	59	45	38	30	31	24	20	17	35	30	27	23
HDS activity[b] at 300 °C	0.40	0.63	1.06	1.70	0.21	0.34	0.56	0.96	0.24	0.42	0.75	1.30

[a] Run-to-run conversion reproducibility = ±15% (e.g., 20 ± 3%). Amount of "active" metals in each run = 0.10 g in all cases. [b] Activity in g of DBT converted/(g of catalyst) h.

the non-sulfur-containing aromatic rings prior to desulfurization, resulting in cyclohexylbenzene. Such aromatic ring saturation requires more costly hydrogen and is, therefore, not desirable. The direct desulfurization and aromatic ring saturation reaction pathways are shown in eqs 1 and 2, respectively. At higher temperatures where mass-transport limitations were not as significant, the activities and selectivities of the Co_6S_8-pillared MoS_2 materials were competitive with the commercial catalysts.

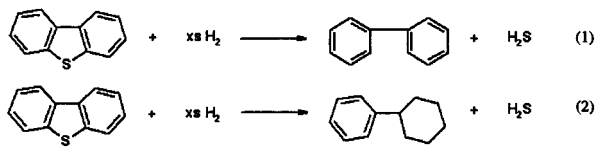

In addition to being competitive with the commercial catalysts, the two Co_6S_8-pillared MoS_2 catalysts were far more active than pristine MoS_2, restacked MoS_2, and $Al_{13}O_4(OH)_{24}(H_2O)_{12}^{7+}$-pillared MoS_2 on a per gram of metal basis. Within experimental error, the two Co_6S_8-pillared MoS_2 materials possessed approximately the same reactivity, so no clear relationship between the amount of the $Co_6S_8(PPh_3)_6$ clusters in the material and reactivity could be determined. The restacked MoS_2 provided a modest conversion and was significantly better than the pristine MoS_2 on a per gram of catalyst basis. Most importantly, if one normalizes the activities by surface area, one finds that the pristine MoS_2, restacked MoS_2, and the two Co_6S_8-pillared MoS_2 materials all possessed very similar reactivities (Figure 15). The large error bars (95% confidence intervals) in Figure 15 are mostly attributable to a high region-to-region variability in the number of near-edge vacancies. When combined with the relatively low conversions observed for the *x*-$[Co_6S_8(PPh_3)_n]-MoS_2-R$ materials (Table 4), our results suggest that, at least in pillared MoS_2 materials, the HDS promotional role of Co is largely structural.

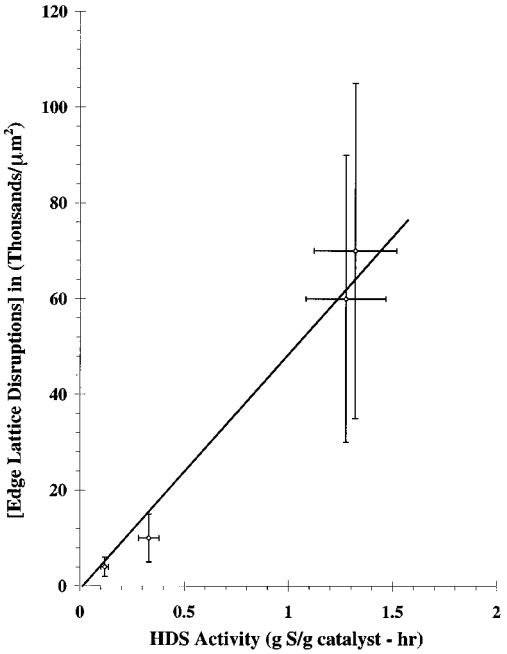

Figure 15. Correlation of HDS activity of pristine MoS_2, restacked MoS_2, $[Co_6S_8(PPh_3)_n]_{0.02}MoS_2$, and $[Co_6S_8(PPh_3)_n]_{0.05}$-$MoS_2$ materials with the surface areas of these materials and the concentrations of roughly 1.0 nm lattice disruptions in these materials. The error bars represent the 95% confidence intervals. The large error bars for the concentration of edge lattice disruptions take into account not only the error associated with variability in the concentration of lattice disruptions within the edge planes but also region-to-region variability in the percentage of edge planes.

Discussion

Transmission Electron Microscopy. Whether or not the intercalated regions would be separated by regions with unexpanded lattice spacings is dependent on the pillaring density and the rigidity of the host lattice. If the cluster loading was sufficiently low and the clusters were uniformly dispersed, then one would expect that the disturbance in the structure of the layered material might be very localized. Conversely, if the cluster loading were near the stoichiometric limit, one would expect the pillaring to separate the layered material over crystal-wide length scales. For MoS_2, a lubricant, the critical pillar concentration is likely higher than for more rigid compounds such as pillared clays.

The presence of Co clusters could be theoretically detected in two ways. Because of the lower atomic number (relative to Mo) and the molecular nature of the clusters, one would certainly expect the Co scattering to be relatively weak in intensity (if detectable) and discrete relative to the MoS_2 layers. For crystals in which the $\{hk0\}$-MoS_2 planes were observed, Co might be detected as discrete scattering centers of the size of the Co_6S_8 core. (The PPh_3 ligands, if still there, would not likely scatter sufficiently to be detected by TEM). As can be seen in Figure 16, the diameter of the Co_6S_8 core is approximately 0.8 nm, whereas the diameter of the $Co_6S_8(PPh_3)_6$ cluster precursors is 1.48 nm.

The encapsulation of the Co cluster expands the MoS_2 lattice spacing only locally for the most part at low Co cluster loadings (0.12 Co atoms per Mo), whereas at intermediate loadings (0.30 Co atoms per Mo), MoS_2 layers were often separated by 0.8 nm for lengths of 5−10 nm. No evidence for Co-containing phases was observed external to MoS_2 domains. In fact, the excellent agreement between the size of the discrete scattering centers as measured by TEM (0.87 nm) with the size of a Co_6S_8 cluster core (0.8 nm) is strong evidence that the clusters were, for the most part, molecularly dispersed throughout the MoS_2 matrix.

The presence of Co_6S_8 clusters could be detected far more easily by the expansion of the $\{00l\}$-1T−MoS_2 planes from 0.615 nm to some larger distance. Such lattice expansion would be consistent with Co cluster intercalation between MoS_2 lamellae near the edges of the MoS_2 layers. The distance associated with such $\{001\}$-$[Co_6S_8(PPh_3)_n]_{0.02}MoS_2$ planes could vary from approximately 1.4 nm (for sections from which the triphenylphosphine ligands have been completely removed) to 2.1 nm, the distance for $\{001\}$-$[Co_6S_8(PPh_3)_n]_{0.02}MoS_2$ planes determined from X-ray diffraction (XRD). Lengths between 1.4 and 2.1 nm would indicate partial loss of the triphenylphosphine ligands. The average distance between layers in the region which appeared to be nearly completely pillared was 1.46 ± 0.10 nm, corresponding to a lattice expansion of 0.78 ± 0.10 nm and confirming that the triphenylphosphine ligands had been completely removed either prior to or during TEM examination. In the case of the $[Co_6S_8(PPh_3)_n]_xMoS_2$ materials, vacuum pumpdown might have evolved the triphenylphosphine ligands. Electron-beam degradation of the triphenylphosphine ligands cannot be ruled out during the first 2 min of the TEM experiments, however.

Several TEM studies of pillared clays have been reported.[53−55] Typically, these have involved the addition of an aluminum Keggin ion, $Al_{13}O_4(OH)_{24}(H_2O)_{12}^{7+}$, into a clay matrix. Gil et al.[54] have reported mean

Table 4. HDS Activities[a]

catalyst	percent conversion (biphenyl selectivity) 400 °C	350 °C	300 °C	250 °C	surface area (m^2/g)
$[Co_6S_8(PPh_3)_x]_{0.02}MoS_2$	85 (50)		38 (61)	15 (7)	26.8
$[Co_6S_8(PPh_3)_x]_{0.05}MoS_2$	88 (52)	61 (48)	42 (41)	12 (25)	30.0
0.02-$[Co_6S_8(PPh_3)_n]$−MoS_2−R	25 (73)	10 (76)	<5 (NM)	<5 (NM)	9.3
0.05-$[Co_6S_8(PPh_3)_n]$−MoS_2−R	30 (70)	15 (48)	<5 (NM)	<5 (NM)	8.9
Al_{13}-pillared MoS_2	6 (89)	<5 (NM)	<5 (NM)	<5 (NM)	10.0
restacked MoS_2	22 (75)	9 (78)	<5 (NM)	<5 (NM)	10.0
pristine MoS_2	8 (88)	<5 (NM)	<5 (NM)	<5 (NM)	5.8
Crosfield 465 (Co−Mo)	82 (80)	56 (91)	20 (85)	<5 (NM)	
Crosfield 504 (Ni−Mo)	98 (44)	58 (46)	27 (76)	10 (55)	

[a] NM = not meaningful (conversion too low that selectivity could not be reliably determined). Run-to-run conversion reproducibility = ±15% (e.g., 20 ± 3%). Amount of "active" metals (Co + Mo) in each run = 0.10 g in all cases.

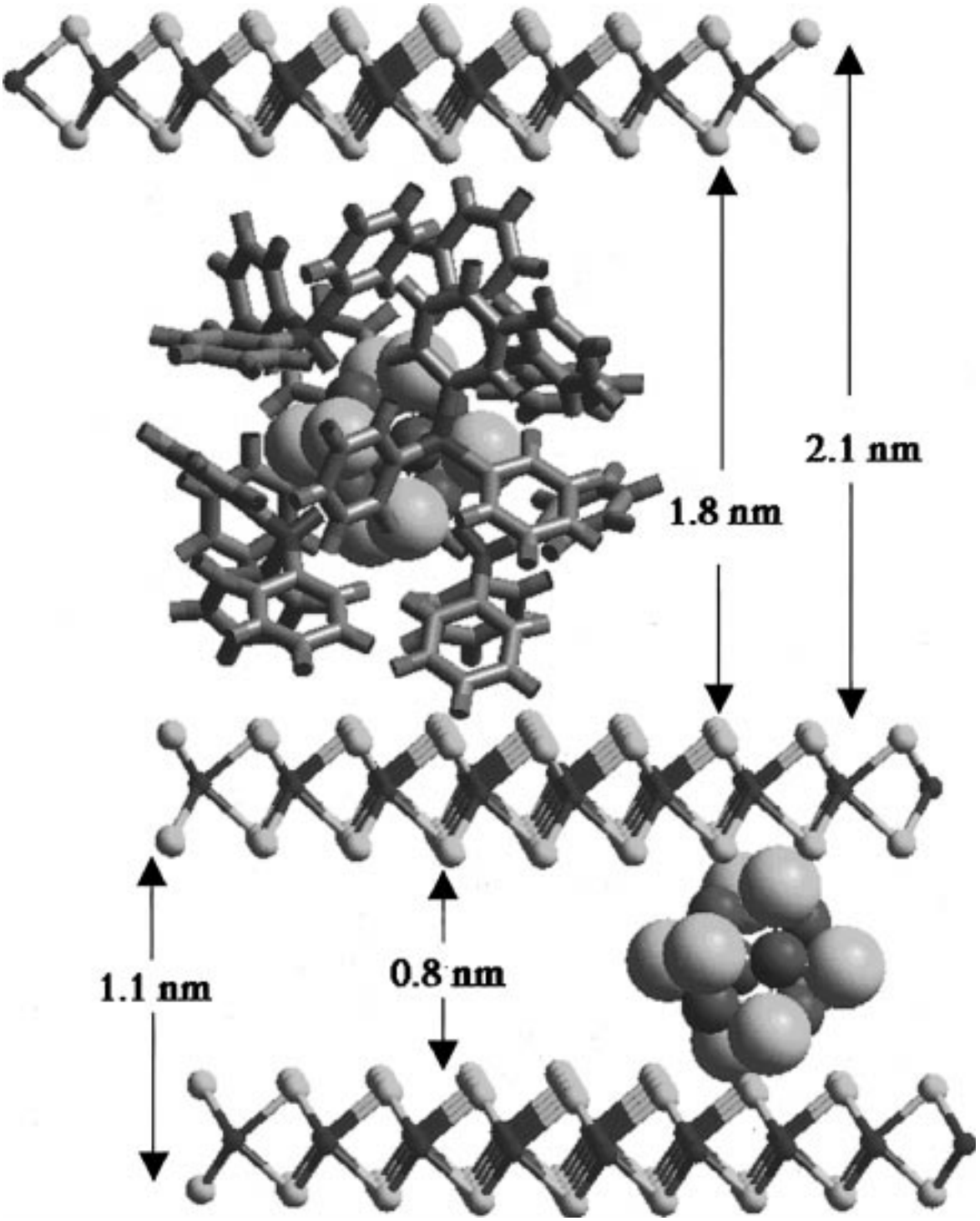

Figure 16. Diagram of a $Co_6S_8(PPh_3)_6$ cluster, the pillaring agent, interspersed between layers of MoS_2.

lattice spacings from TEM of 0.3−0.5 nm less than those reported from XRD for Keggin ion-pillared clays. They attributed these decreased lattice spacings to dehydration of the water-soluble Keggin ion during vacuum pumpdown in the TEM specimen chamber. Perhaps for this reason, the use of TEM to study pillared materials has been quite limited. Like previous workers studying the intercalation of the Keggin ion into pillared clays, we were unable to detect the Keggin ion in $Al_{13}O_4(OH)_{24}(H_2O)_{12}^{7+}-MoS_2$ directly as a scattering center but, like Gil,[54] we were able to see a distribution of lattice expansions due to its presence.

X-ray diffraction suggests the presence of pillared $[Co_6S_8(PPh_3)_n]_{0.02}MoS_2$ and little if any unpillared MoS_2.[46] However, the unpillared MoS_2 edge lattice spacing overlaps with one of the XRD peaks for the pillared $[Co_6S_8(PPh_3)_n]_{0.02}MoS_2$, so interpretation based solely on XRD is somewhat ambiguous. Partial population of unpillared MoS_2 edge sites with the Co clusters would destroy much of the coherence in the X-ray diffraction.

(53) Rightor, E. G.; Pinnavaia, T. J. *Ultramicroscopy* **1987**, *22*, 159.
(54) Gil, A.; Diaz, A.; Montes, M.; Acosta, D. R. *J. Mater. Sci.* **1994**, *29*, 4927.
(55) Witkowski, S.; Dyrek, K.; Sojka, Z.; Djéga-Mariadassou, G.; Fijal, J.; Klapyta, Z. *Clay Miner.* **1994**, *29*, 743.

Thus, the regions that are completely pillared would be expected to give rise to most of the signal in X-ray diffraction patterns.

The major advantages of the use of TEM over XRD for studying pillared materials are that one can determine the degree and uniformity of the pillaring in localized regions. As has been shown in the micrographs, there were distinct heterogeneities in the degree of pillaring of MoS_2 not visible by XRD. Moreover, in cases where the pillaring is partial, XRD may give an incorrect interpretation of the pillaring behavior. In our case, TEM suggests that the disruptions in the MoS_2 lattice were highly localized at the surface, whereas XRD suggests that the predominant structure is that of a perfectly pillared material.[46] Of course, the two techniques probe different regions and consequently provide complementary information. Only the edges were observed by TEM, while XRD samples the entire material. We suggest that the presence of large internal areas of pillared MoS_2 could be observed by examination of a microtomed, resin-embedded sample.

HDS Activity. The activities of the Co_6S_8-pillared molybdenum disulfides at low temperatures ($\leq$300 °C) were the highest per gram of catalyst of the many materials that we have tested and were still slightly more active than commercially available sulfides on a per gram of metal basis. This activity benefit is partially offset by a relatively low selectivity to biphenyl, implying a more significant hydrogenation function for the pillared materials as compared to the commercial catalysts. The effect of mass transport at low severity HDS conditions, while very significant, was also less important for the Co_6S_8-pillared MoS_2 than for the commercial catalysts, suggesting that the pillaring may have enhanced the accessibility of the active sites.

The Co_6S_8-pillared molybdenum disulfides were only active, however, once the triphenylphosphine ligands had been evolved. Following a 300 °C H_2 reduction, the evolution of these ligands was detected readily by a color change in the KOH scrubbing solution. This initially clear solution, meant to trap H_2S as K_2S precipitate, turned bright orange. Pyrolysis mass spectroscopy experiments[46] indicated that the majority of the volatile product from the Co_6S_8-pillared molybdenum disulfides were phosphine sulfide fragments (both PhPS and Ph_2-PS) that, when combined with the fact that only triphenylphosphine was observed during pyrolysis of the neat cluster, suggests that the phosphines attacked the MoS_2 layers by extracting sulfur as they departed from the solid. Extraction of sulfur from the MoS_2 layers during thermal pretreatment prior to catalysis or during e-beam exposure in the TEM would create vacancies at which the Co_6S_8 cluster cores would be preferentially stabilized; such a mechanism would certainly help to explain the fact that the Co_6S_8 cluster cores did not aggregate into large cobalt sulfide domains.

The sulfur extraction during the evolution of the triphenylphosphine ligands creates sulfur anion vacancies, which have long been associated with HDS-active sites. Certainly, there are localized disruptions in the MoS_2 lattice (in Figures 7, 8, and 10) which are about 0.9 nm. These disruptions are too big to be the sulfur anion vacancies that have been associated with HDS activity and are more likely associated with remnants from the Co_6S_8 cluster fragments. Nevertheless, the removal of Ph_3P ligands may be an interesting activation step for introducing additional reactivity in the MoS_2 layers.

Structure−Reactivity Relationships. Some of the local lattice disruptions in MoS_2 edge structures observed in this work, such as those in Figures 7, 8, and 10, might be due to defects induced by cobalt-containing clusters. These local lattice disruptions seem barely present, if at all, in the restacked and pristine MoS_2 materials, as compared to the significant number in the Co cluster-loaded materials. Although screw dislocations and Moiré fringes are commonly observed in MoS_2 catalysts,[56−60] the appearance of circular scattering regions (in 2-D) of 0.5−1.5 nm, to our knowledge, has not been reported for unpromoted MoS_2 and was not observed in our work for either the pristine nor the restacked MoS_2 materials. However, structures such as those in Figures 7, 8, and 10 in our paper have been reported in Figure 9 of a recent paper by Chianelli et al.[59] for bulk MoS_2 doped by 1 wt % Co.

In the Co_6S_8-pillared materials, both the 1T and 2H forms of MoS_2 were detected. The 1T form, more common in our materials but not as thermodynamically stable as the 2H form, has a highly distorted sulfur close-packed layer[42,43] and is related to that of highly HDS active ReS_2.[59] Chianelli et al.[59] also reported 1T superlattices within their Co-doped MoS_2 single crystals. They concluded that near-edge Co distorts the sulfur close-packed layer, inducing lattice strain and a slight rotation of one sulfur close-packed layer with respect to another. This rotation further results in regular Moiré fringes that have been observed in the micrographs of several researchers.[59,60] This Co-induced lattice strain is absent away from the edges of Co-doped MoS_2 single crystals,[60] as the intercalation of Co into Mo sulfides is mostly a surface phenomenon, with the deepest penetration of Co being only a few layers.[61]

Daage and Chianelli[1] have argued that the "rim" sites, in addition to possessing the desulfurization capability of "edge" sites, are efficient at hydrogenation. If Daage and Chianelli's rim-edge model[1] is correct, a restacked MoS_2 would be expected to be more active but less selective for direct desulfurization of dibenzothiophene to biphenyl because the exfoliation and flocculation processes decrease the basal plane area effectively increasing the rim/basal plane ratio. The restacked MoS_2 gave rise to a higher conversion and a lower hydrogen selectivity than the pristine MoS_2. The Co_6S_8-pillared MoS_2 catalysts produced higher conversions and lower hydrogen selectivities than either the restacked or pristine MoS_2 materials. On a surface area-specific activity basis, however, the activities of the Co_6S_8-pillared MoS_2 catalysts and the activities of the pristine

(56) Srinivasan, S.; Datye, A. K.; Peden, C. H. F. *J. Catal.* **1992**, *137*, 513.
(57) Stockmann, R. M.; Zandbergen, H. W.; van Langeveld, A. D.; Moulijn, J. A.*J. Mol. Catal. A−Chem.* **1992**, *102*, 147.
(58) Pedraza, F.; Cruz-Reyes, J.; Acosta, D.; Yañez, M. J.; Avalos-Borja, M.; Fuentes, S. *J. Phys.: Condens. Matter* **1993**, *5*, A219.
(59) Cruz-Reyes, J.; Avalos-Borja, M.; Farías, M. H.; Fuentes, S. *J. Catal.* **1992**, *137*, 232.
(60) Chianelli, R. R.; Ruppert, A. F.; José-Yacamán, M.; Vázquez-Zavala, A. *Catal. Today* **1995**, *23*, 269.
(61) Topsøe, N.-Y.; Topsøe, H.; Sørensen, O.; Clausen, B. S.; Candia, R. *Bull. Soc. Chim. Belg.* **1984**, *93*, 727.

and restacked MoS_2 materials were essentially constant (Figure 15). In addition, the concentration of these 0.9 nm disruptions in the MoS_2 lattice also roughly correlates with the activity of the material (Figure 15). The large error bars (95% confidence intervals) for the concentration of edge lattice disruptions take into account not only error associated with variability in the concentration of lattice disruptions within the edge planes but also region-to-region variability in the percentage of edge planes, the latter of which is more significant. Despite the large uncertainty, these results suggest that the exfoliation and flocculation processes increase the MoS_2 surface area, thereby increasing hydrogenation capability, and that the presence of Co clusters both decreases the degree of stacking while increasing the degree of hydrogenation. In this respect, Co props apart MoS_2 layers, thereby increasing dispersion and hydrogenation activity in a manner consistent with Daage and Chianelli's "rim-edge" model[1] of hydrodesulfurization active sites, and acts as a structural promoter in the current catalyst.[62]

Conclusions

Evidence for intercalation of $Co_6S_8(PPh_3)_6$ clusters into MoS_2 was observed by both expansion of the {00*l*}-1T−MoS_2 *d* spacing and by observation of discrete scattering centers. Both the size of the discrete scattering centers and the observed average lattice expansion between MoS_2 layers were consistent with the size expected for the Co_6S_8 cores of the $Co_6S_8(PPh_3)_6$ clusters, indicating that the phosphine ligands had been nearly completely removed. Transmission electron microscopy revealed not only domains of crystal-wide pillaring but also large regions of randomly pillared MoS_2. The Co_6S_8 cluster remnants were readily visible along the edges of {00*l*}-1T−MoS_2 edge planes.

The activities of the Co_6S_8-pillared MoS_2 materials were competitive with those of commercial, sulfided Co−Mo and Ni−Mo hydrotreating catalysts and even slightly superior at low temperatures. However, the selectivity to biphenyl was relatively poor compared to the commercial catalysts. The HDS reactivity results are consistent with the Daage−Chianelli rim-edge model[1].

Acknowledgment. This work was performed under the auspices of the U.S. Department of Energy, Office of Fossil Energy-Bartlesville under Contract W-31-109-ENG-38. Financial support from the National Science Foundation Chemistry Research Group (CHE-96-33798) for the Michigan State authors is gratefully acknowledged. This work made use of TEM facilities at the Electron Microscopy Center for Materials Research at Argonne National Laboratory. We thank Professor Thomas J. Pinnavaia (MSU) and Dr. Roseann Csencsits (Argonne) for fruitful discussions.

CM970592T

(62) Lindner, J.; Villa Garcia, M. A.; Sachdev, A.; Schwank, J. W. *J. Chem. Soc., Chem. Commun.* 1989, 1834.